Theoretical Mechanistic Study on the Ion−Molecule Reactions of CCN^+/CNC^+ with H_2S

Yu-guo Tao, Yi-hong Ding,* Jian-jun Liu, Ze-sheng Li, Xu-ri Huang, and Chia-Chung Sun

State Key Laboratory of Theoretical and Computational Chemistry, Institute of Theoretical Chemistry, Jilin University, Changchun 130023, People's Republic of China

Received: October 18, 2001; In Final Form: January 24, 2002

A detailed [$C_2H_2NS^+$] potential energy surface in singlet, including 45 minimum isomers and 57 transition states, is built up at the B3LYP/6-311G(d,p) and CCSD(T)/6-311G(2df,p) (single-point) levels in order to explore the mechanisms of the important ion−molecule reactions between CCN^+/CNC^+ and H_2S. For the reactions of both CCN^+ and CNC^+ toward H_2S, product $HCS^+ + HNC$ may be the most abundant followed by the much less $HCNH^+ + CS$ and then $HCS^+ + HCN$. Significant discrepancies on the product distributions are found between our calculated results and previous experimental finding. On the other hand, the reaction of $HCNH^+ + CS$ to form $HCS^+ + HCN/HNC$ is also considered by the [$C_2H_2NS^+$] PES. For such reaction, the barrierless association may lead to the adduct $HNC(H)CS^+$, while the proton-transfer may barrierlessly lead to product $HCS^+ + HCN/HNC$ via the hydrogen-bound complexes $SCH\cdots NCH^+/SCH\cdots CNH^+$. The computations reported in this paper may represent the first theoretical study on the chemical reactivity of the C_2N^+ ion and may thus provide a useful guide for understanding the mechanisms of the other analogous reactions such as those of C_2N^+ with H_2O, CH_4, NH_3, CH_3OH, etc. The present calculations may also provide useful information for future laboratory investigations on the $HCNH^+ + CS$ reactions that have not been previously studied. Interstellar implications of the title reactions are discussed.

1. Introduction

Gas-phase ion−molecule reactions have been considered to play a crucial role in the interstellar chemistry.[1−3] Such reactions are generally very fast and may thus be very effective in synthesizing novel molecules or ions. Many simple synthetic models associated with the ion−molecule reactions have been successfully developed.[2]

One ion that has attracted considerable attention is C_2N^+. It has been predicted to be one of the most abundant molecular ions in the interstellar medium.[4] Its two isomeric forms, CNC^+ and CCN^+ (higher-energy), could be selectively generated via the important reactions $C^+ + HCN \rightarrow CNC^+ + H$ and $C^+ + HNC \rightarrow CCN^+ + H$[5] or by the electron impact on C_2N_2, CH_3CN, CH_3NC, and HC_3N.[6,7] The chemical reactivity of C_2N^+ has been explored in several laboratory studies.[8,9] Particularly, Bohme et al. carried out a selected-ion flow tube (SIFT) study on the C_2N^+ reactions toward a number of neutral species including N_2, CO, HCN, C_2N_2, N_2O, H_2O, H_2S, CH_4, NH_3, etc. Their results not only gave further support to the existence of two C_2N^+ isomers with distinct reactivity but also indicated that these C_2N^+ reactions could lead to many novel species such as those involving C−S, C−O, and C−N bonding. Many theoretical investigations have been devoted to the structures and spectroscopic constants of the CCN^+ and CNC^+ species.[10,11]

In sharp contrast, no theoretical studies about the C_2N^+ reactions have been reported, to our best knowledge. In the present article, we focus on the gas-phase mechanism of the C_2N^+ reaction with H_2S, which is a polar molecule in the interstellar space and its reactions have been identified as important in sulfur combustion under rich conditions[12] and the prototype for sulfur oxidation in the atmosphere.[13,14] The chemistry of the reaction of $C_2N^+ + H_2S$, together with the analogous reactions of C_2N^+ with H_2O, CH_4, NH_3, etc., is directed toward the synthesis of carbenes such as :CO, :CS, etc. in interstellar gas clouds.[15] Only one previous experimental measurement on the product distributions of the $C_2N^+ + H_2S$ reaction has been reported. In Bohme et al.'s SIFT experiments,[8] the branching ratios were determined to be $CHS^+ + CHN$ (95%) and $C_2NS^+ + H_2$ (5%) for the $CNC^+ + H_2S$ reaction; they pointed out that the former product ion may be achieved by S−H bond insertion and the latter will result from S-atom abstraction. No product distribution measurement has been reported for the $CCN^+ + H_2S$ reaction. It should be pointed out that in the above experiment, the real chemical formula of CHS^+ (HCS^+ or HSC^+) and CHN (HCN or HNC) could not be determined. It seems quite difficult to speculate the detailed mechanism of such ion−molecule reactions, which may involve complex isomerization and dissociation channels. Therefore, a detailed theoretical characterization on the [$C_2H_2NS^+$] potential energy surface of the $C_2N^+ + H_2S$ reaction is very desirable. Such results are presented in section 3.1.

As another important goal, we attempt to investigate the ion−molecule reactions between $HCNH^+$ and CS, which are also related to the [$C_2H_2NS^+$] potential energy surface. The $HCNH^+$ has been detected in interstellar space and has been considered to be present in considerable abundance. To our knowledge, the $HCNH^+$ with CS reaction has not been studied up to now either experimentally or theoretically. The proton transfer from $HCNH^+$ to CS may lead to HCN/HNC and HCS^+, which are also important and abundant species in interstellar space. On the other hand, the barrierless association to the adduct $HNC(H)CS^+$, which may lead to $SC(H)CNH^+$ via a H-shift between two adjacent C-atom and then disassociate to $HCS^+ + HNC$ directly, may thus display association-elimination channels. The two process types will be theoretically discussed in section 3.2.

10.1021/jp013892d CCC: $22.00
Published on Web 02/28/2002

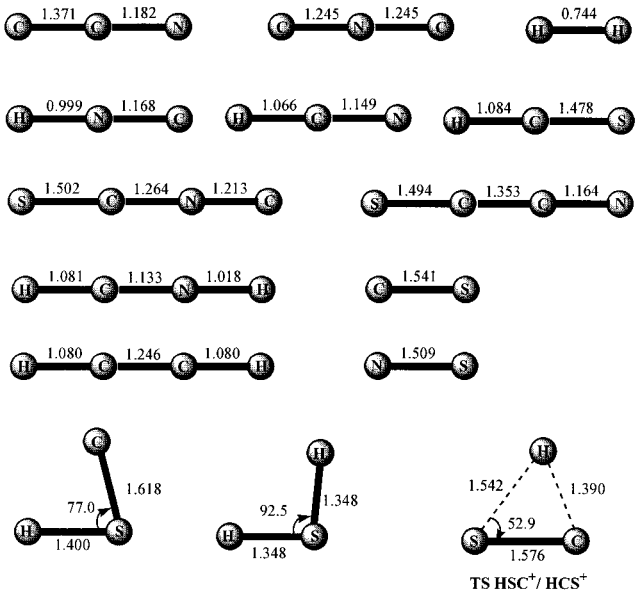

Figure 1. B3LYP/6-311G(d,p) optimized geometries for reactant and products. Bond lengths are in angstroms and angles in degrees.

2. Computational Methods

All computations are carried out using the GAUSSIAN98 program package.[16] The optimized geometries and harmonic frequencies of the reactant, products, local minima and transition states are obtained at the B3LYP/6-311G(d,p) level. Single-point calculations are performed at the CCSD(T)/6-311G(2df,p) level at the B3LYP/6-311G(d,p)-optimized geometries. The B3LYP/6-311G(d,p) zero-point vibration energy (ZPVE) is also included. To confirm whether the obtained transition states connect the right reactants and products, the intrinsic reaction coordinate (IRC) calculations are performed at the B3LYP/6-311G(d,p) level.

3. Results and Discussion

For the present $C_2H_2NS^+$ system, 45 intermediate isomers and 57 transition states are located. Figure 1 shows the structures of the reactants and various dissociation products. Figures 2 and 3 depict the structures of the isomers and transition states, respectively. The total and relative energies of various dissociation products are listed in Table 1, while those of the isomers and transition states are given in Tables 2 and 3. The harmonic vibration frequencies (cm^{-1}) for the transition states are listed in Table 4 at the B3LYP/6-311G(d,p) level, from which we can see that there is only one negative vibration frequency in each transition state. It should be noted that the cation HSC^+ with linear skeleton cannot be found and there are significant differences between cations HCS^+ and HSC^+, in which the relative energy of HSC^+ is 75.8 kcal/mol higher than that of HCS^+ at the CCSD(T)/6-311G(2df,p)//B3LYP/6-311G(d,p) level. A transition state between HCS^+ and HSC^+ is therefore located whose relative energy is only 0.5 kcal/mol higher than that of HSC^+. Namely, it is easier for the very unstable ion HSC^+ to change into the more stable ion HCS^+ and it is very difficult to generate products $\mathbf{P_6}$ ($HSC^+ + HCN$) and $\mathbf{P_7}$ ($HSC^+ + HNC$), which can isomerize to the corresponding products $\mathbf{P_2}$ ($HCS^+ + HCN$) and $\mathbf{P_3}$ ($HCS^+ + HNC$) almost barrierlessly.

By means of the appropriate isomers, transition states and products, the schematic potential energy surfaces (PES) for $CCN^+ + H_2S$ and $CNC^+ + H_2S$ are plotted in Figure 4a,b, respectively. Note that the energy of $CCN^+ + H_2S$ is set to zero as a reference for the other species. In the following discussion, the symbol **TS*m*/*n*** is used to denote the transition state connecting the isomers ***m*** and ***n***. Unless otherwise stated, the CCSD(T)/6-311G(2df,p)//B3LYP/6-311G(d,p) + ZPVE relative energies are used throughout.

3.1. $C_2N^+ + H_2S$ Reaction. *3.1.1. Association.* The C_2N^+ ion has two isomeric forms. The ground-state structure is CNC^+ and the higher-energy one is CCN^+, lying 24.7 kcal/mol above. For the CCN^+ and CNC^+ forms, the initial association with H_2S can most favorably generate the terminal C-attack adduct H_2SCCN^+ (**1**) (−72.2) and H_2SCNC^+ (**6**) (−65.0), respectively. For the $CCN^+ + H_2S$ reaction, the terminal N-attack may form adduct H_2SNCC^+ (**12**) (−33.3), which is thermodynamically much less favorable than **1**. No association barriers can be found for the formation of **1**, **6**, and **12**. Note that the values in parentheses are relative energies in kcal/mol with reference to $\mathbf{R_1}$ ($CCN^+ + H_2S$) (0.0).

3.1.2. Isomerization and Dissociation. As shown in Figure 4a, the high-energy adduct H_2SNCC^+ (**12**) for the $CCN^+ + H_2S$ reaction can either take a 1,2-H-shift to isomer HSN(H)-CC^+ (**13**) (−49.7) or take a 1,4-H-shift to isomer $HSNCCH^+$ (**14**) (−100.6). Yet, since **TS12/13** (1.6) and **TS12/14** (−4.1) lie well above corresponding H-shift transition states **TS1/2** (−52.5) and **TS1/3** (−36.5) from the C-attack adduct H_2SCCN^+ (**1**), such processes are surely less competitive and unfeasible at low temperatures, which will not be considered further.

TABLE 1: Total (au) and Relative Energies in Parentheses (kcal/mol) as Well as Those Including Zero-Point Vibration Energies (kcal/mol) of the Reactant and Products for the $C_2N^+ + H_2S$ Reaction at Singlet[a]

species	B3LYP/6-311G(d,p)	CCSD(T)/6-311G(2df,p)	CCSD(T)/6-311G(2df,p) + ΔZPVE
$\mathbf{R_1}$ ($CCN^+ + H_2S$)	−529.8001955/(0.0)	−529.0414982/(0.0)	0.0
$\mathbf{R_2}$ ($CNC^+ + H_2S$)	−529.8423096/(−26.4)	−529.0807111/(−24.6)	−24.7
$\mathbf{P_1}$ ($HCNH^+ + CS$)	−529.9793213/(−112.4)	−529.2266638/(−116.2)	−112.6
$\mathbf{P_2}$ ($HCS^+ + HCN$)	−530.0094523/(−131.3)	−529.2589419/(−136.4)	−131.8
$\mathbf{P_3}$ ($HCS^+ + HNC$)	−529.9858233/(−115.4)	−529.2343001/(−117.3)	−115.8
$\mathbf{P_4}$ ($SCCN^+ + H_2$)	−529.9836616/(−115.2)	−529.2269808/(−116.4)	−115.9
$\mathbf{P_5}$ ($SCNC^+ + H_2$)	−529.9652774/(−103.6)	−529.2057813/(−103.1)	−103.1
$\mathbf{P_6}$ ($HSC^+ + HCN$)	−529.8898953/(−56.3)	−529.1381798/(−60.7)	−59.4
$\mathbf{P_7}$ ($HSC^+ + HNC$)	−529.8662663/(−41.5)	−529.1135380/(−45.2)	−44.5
$\mathbf{P_8}$ ($HCCH^+ + NS$)	−529.8401555/(−25.1)	−529.0782024/(−23.0)	−19.6
$\mathbf{P_9}$ ($SCHCN^+ + H$)	−529.8958989/(−60.0)	−529.1362438/(−59.5)	−59.4
$\mathbf{P_{10}}$ ($SCHNC^+ + H$)	−529.8722725/(−45.2)	−529.1100180/(−43.0)	−43.2
[a]**TS HSC^+/HCS^+**	−436.4344285/(2.2)	−435.8687181/(1.7)	0.5

[a] The values in parentheses are relative energies with reference to HSC^+ (0.0).

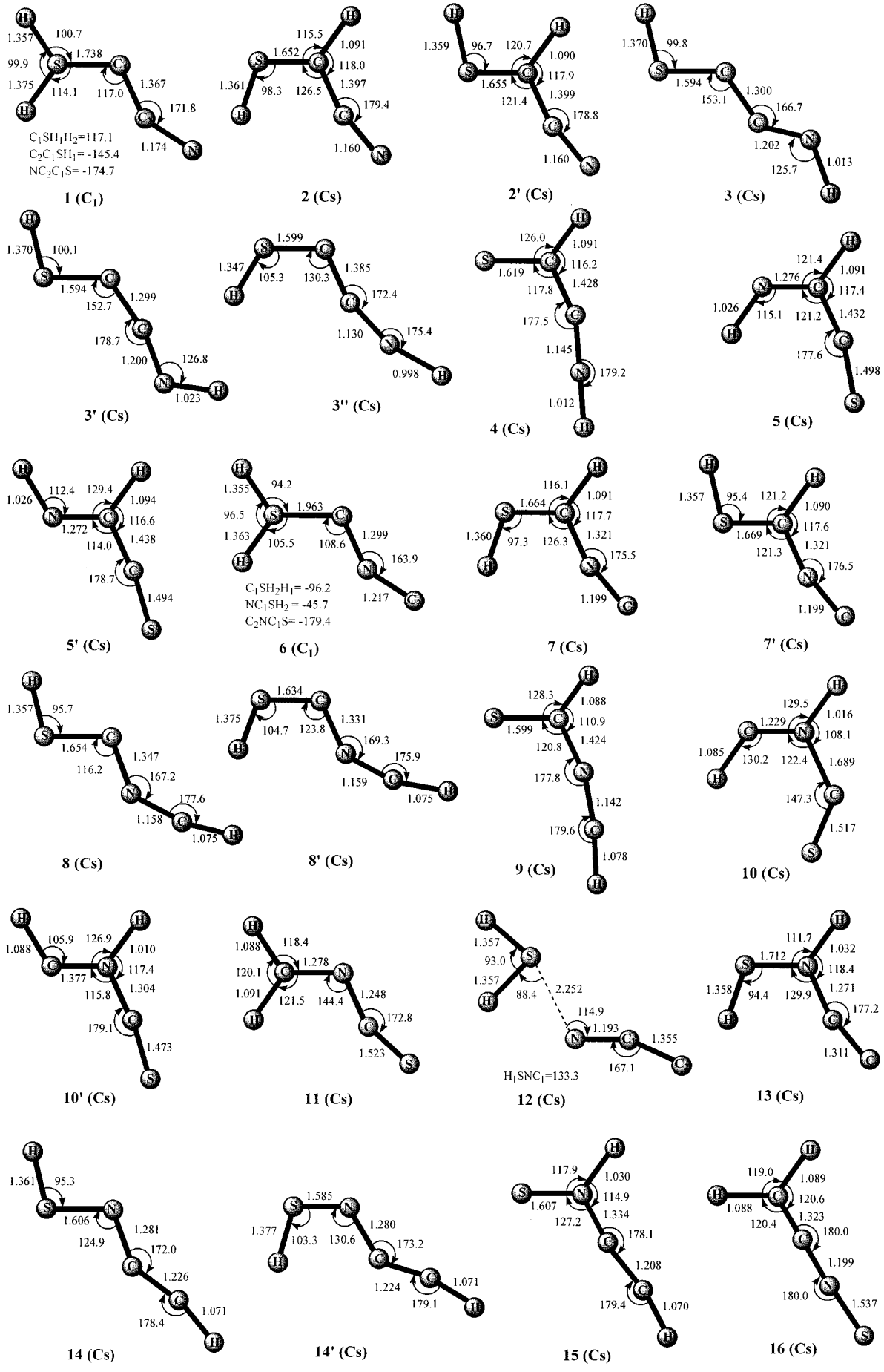
1 (C1)
2 (Cs)
2' (Cs)
3 (Cs)
3' (Cs)
3'' (Cs)
4 (Cs)
5 (Cs)
5' (Cs)
6 (C1)
7 (Cs)
7' (Cs)
8 (Cs)
8' (Cs)
9 (Cs)
10 (Cs)
10' (Cs)
11 (Cs)
12 (Cs)
13 (Cs)
14 (Cs)
14' (Cs)
15 (Cs)
16 (Cs)

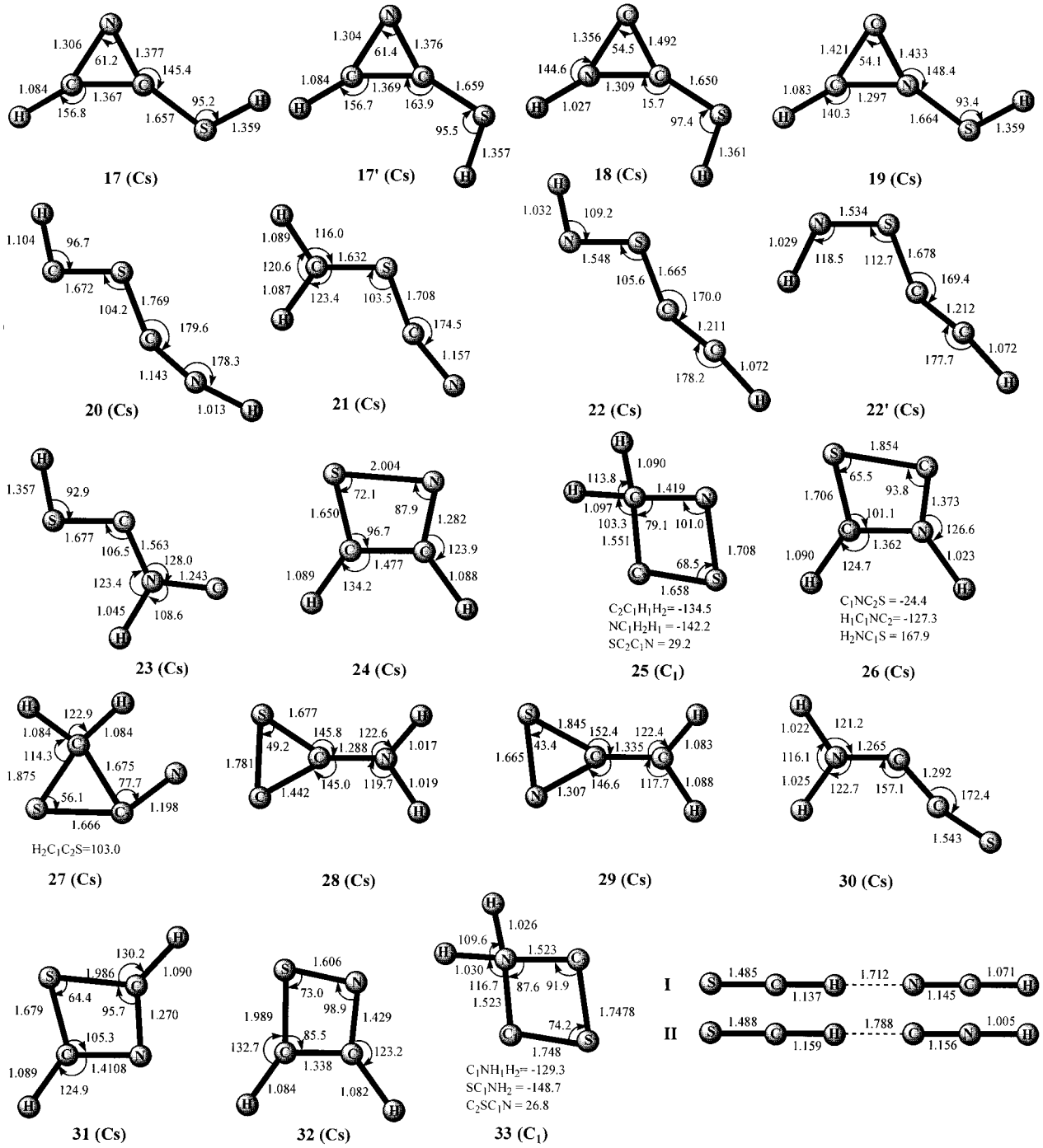

Figure 2. B3LYP/6-311G(d,p) optimized geometries for $C_2H_2NS^+$ isomers. Bond lengths are in angstroms and angles in degrees.

From the lower-energy adduct H_2SCCN^+ (**1**), the most important pathways for the $\mathbf{R_1}$ ($CCN^+ + H_2S$) reaction are

Path $\mathbf{R_1P_3}$: $\mathbf{R_1} \rightarrow H_2SCCN^+$ (**1**) $\rightarrow HSC(H)CN^+$ (**2**) $\rightarrow$ $SC(H)CNH^+$ (**4**) $\rightarrow \mathbf{P_3}$ ($HCS^+ + HNC$)

Path $\mathbf{R_1P_2}$: $\mathbf{R_1} \rightarrow H_2SCCN^+$ (**1**) $\rightarrow HSC(H)CN^+$ (**2**) $\rightarrow$ $SC(H)CNH^+$ (**4**) $\rightarrow \mathbf{P_2}$ ($HCS^+ + HCN$)

Path $\mathbf{R_1P_1}$: $\mathbf{R_1} \rightarrow H_2SCCN^+$ (**1**) $\rightarrow HSC(H)CN^+$ (**2**) $\rightarrow$ $SC(H)CNH^+$ (**4**) $\rightarrow SCC(H)NH^+$ (**5**(**5′**)) $\rightarrow$ $\mathbf{P_1}$ ($HCNH^+ + CS$)

As shown in Figure 4a, the other pathways associated with **2** and **3** are much less competitive than the above three pathways. For simplicity, we will not list them out. **Path $\mathbf{R_1P_3}$**, **Path $\mathbf{R_1P_2}$**, and **Path $\mathbf{R_1P_1}$** may be kinetically more favorable than other product channels, considering the relative energy and entropic value of **TS1/2** (−52.5 and 0.0692 kcal/mol), **TS1/3** (−36.5 and 0.0675 kcal/mol), and **TS1/P4** (−40.4 and 0.0699 kcal/mol), using the Arrhenius formula $k = (KT)/(h)e^{\Delta S/R}e^{-\Delta E/RT}$, where k, ΔS, and ΔE denote the rate constants, entropy differences, and barrier heights and the ratios of $k_{\mathbf{1\rightarrow 2}}/k_{\mathbf{1\rightarrow 3}}$, and $k_{\mathbf{1\rightarrow 2}}/k_{\mathbf{1\rightarrow P4}}$ are 1.2×10^{12} and 5.2×10^{8}, respectively. Although these values are rather rough, it is clear that the formation channel of isomer **2** is much competitive than **3** and the direct disassociation channel of $\mathbf{P_4}$ ($SCCN^+ + H_2$), qualitatively. Also, **Path $\mathbf{R_1P_3}$**

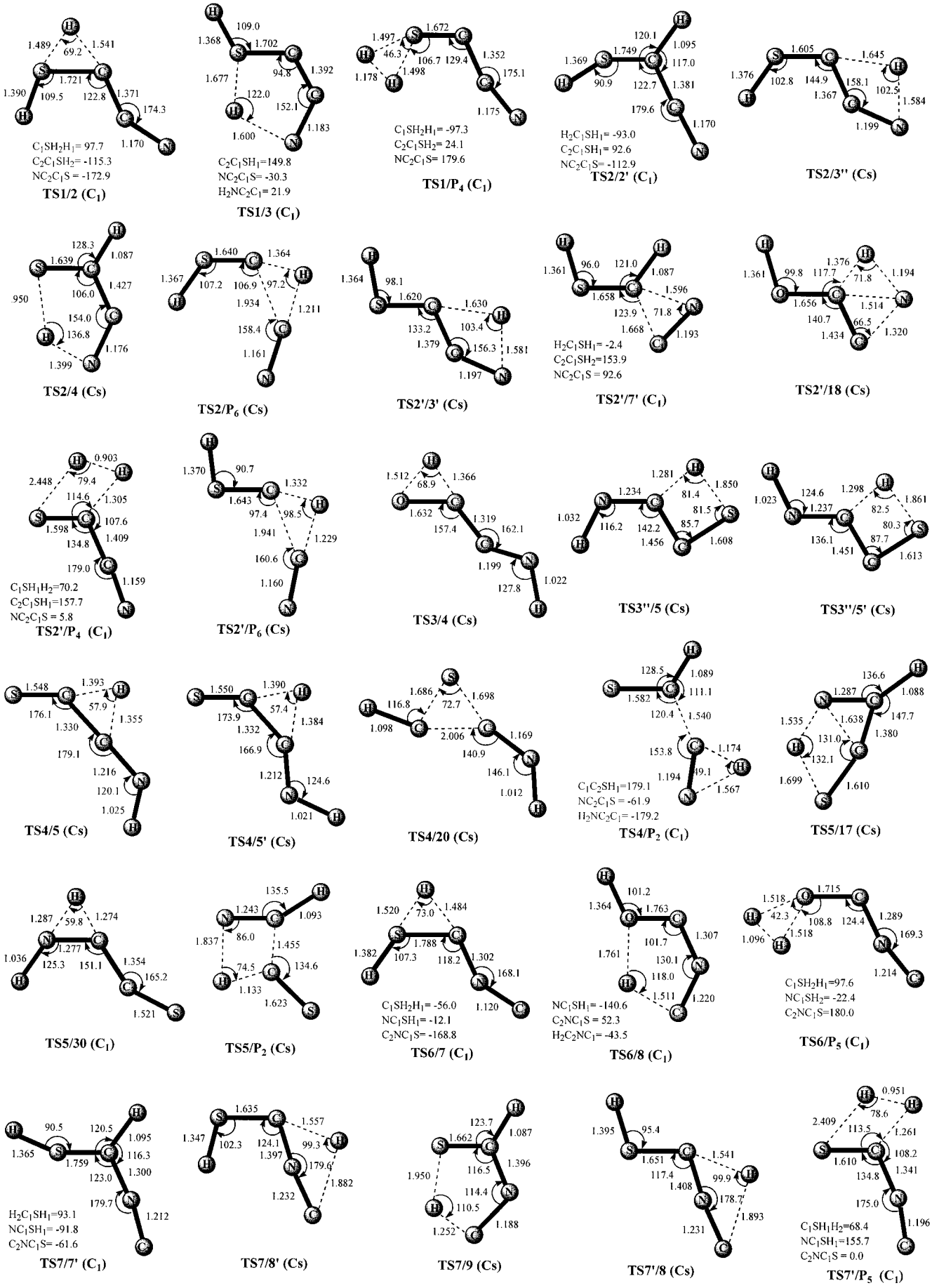
C1SH2H1= 97.7
C2C1SH2= -115.3
NC2C1S = -172.9
TS1/2 (C1)
C2C1SH1=149.8
NC2C1S= -30.3
H2NC2C1= 21.9
TS1/3 (C1)
C1SH2H1= -97.3
C2C1SH2= 24.1
NC2C1S= 179.6
TS1/P4 (C1)
H2C1SH1= -93.0
C2C1SH1= 92.6
NC2C1S= -112.9
TS2/2' (C1)
TS2/3'' (Cs)
TS2/4 (Cs)
TS2/P6 (Cs)
TS2''/3' (Cs)
H2C1SH1= -2.4
C2C1SH2=153.9
NC2C1S = 92.6
TS2''/7' (C1)
TS2''/18 (Cs)
C1SH1H2=70.2
C2C1SH1=157.7
NC2C1S = 5.8
TS2'/P4 (C1)
TS2'/P6 (Cs)
TS3/4 (Cs)
TS3''/5 (Cs)
TS3''/5' (Cs)
TS4/5 (Cs)
TS4/5' (Cs)
TS4/20 (Cs)
C1C2SH1=179.1
NC2C1S = -61.9
H2NC2C1= -179.2
TS4/P2 (C1)
TS5/17 (Cs)
TS5/30 (C1)
TS5/P2 (Cs)
C1SH2H1= -56.0
NC1SH1= -12.1
C2NC1S= -168.8
TS6/7 (C1)
NC1SH1= -140.6
C2NC1S = 52.3
H2C2NC1= -43.5
TS6/8 (C1)
C1SH2H1=97.6
NC1SH2= -22.4
C2NC1S=180.0
TS6/P5 (C1)
H2C1SH1=93.1
NC1SH1= -91.8
C2NC1S= -61.6
TS7/7' (C1)
TS7/8' (Cs)
TS7/9 (Cs)
TS7'/8 (Cs)
C1SH1H2=68.4
NC1SH1=155.7
C2NC1S = 0.0
TS7'/P5 (C1)

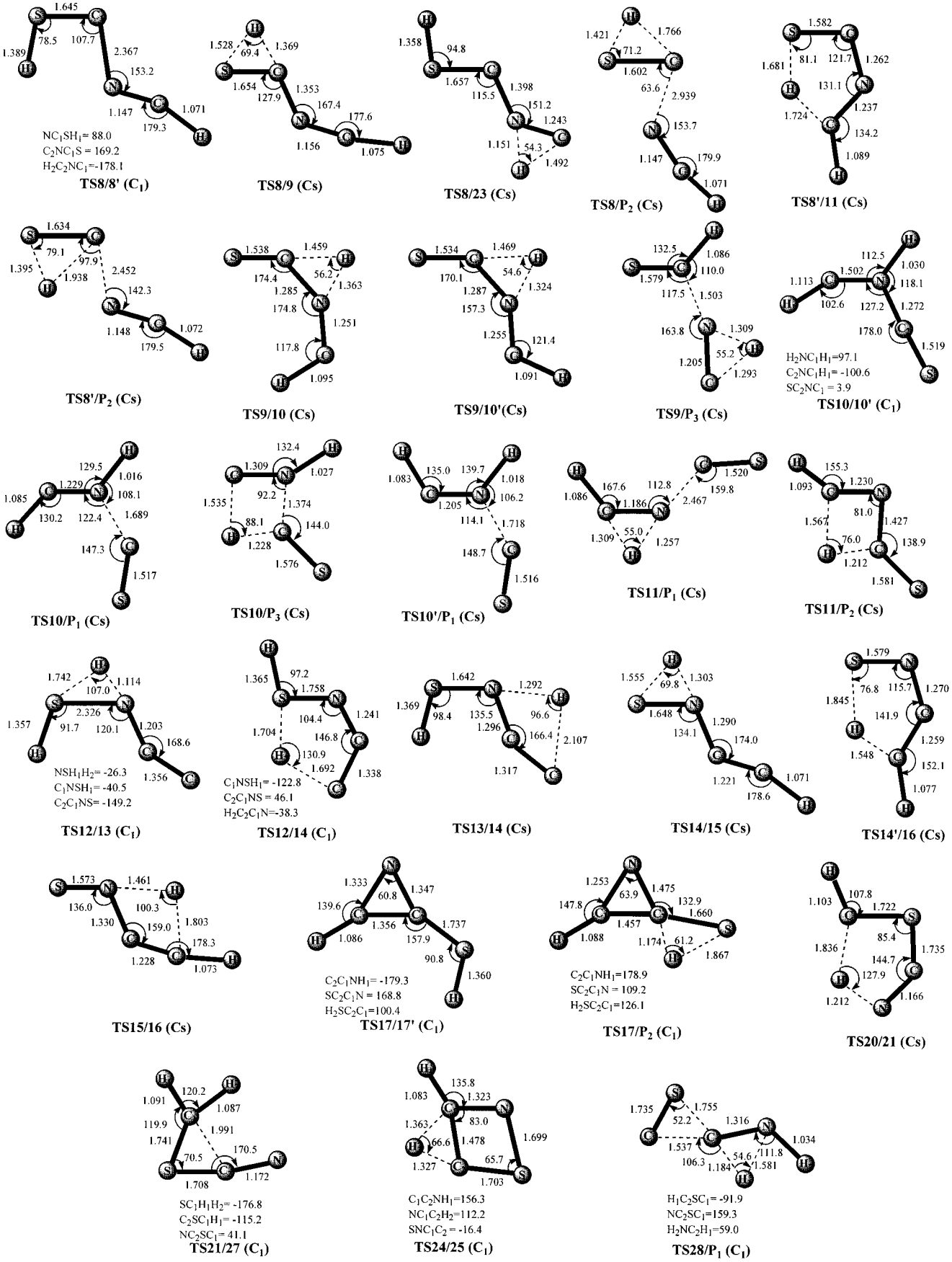

Figure 3. B3LYP/6-311G(d,p) optimized geometries for $C_2H_2NS^+$ transition states. Bond lengths are in angstroms and angles in degrees.

may be much more competitive than **Path R_1P_2** and **Path R_1P_1**, since no barrier is found for the dissociation of **4** to P_3 and P_3 (−116.9) is considerably lower in energy than **TS4/P_2** (−90.7), **TS4/5** (−102.6), and **TS4/5′** (−104.2). Furthermore, **Path R_1P_2** may be kinetically less feasible than **Path R_1P_1** due to the energy barrier heights of **TS4/P_2**, **TS4/5**, and **TS4/5′**.

TABLE 2: Total (au) and Relative Energies in Parentheses (kcal/mol) as Well as Those Including Zero-Point Vibration Energies (kcal/mol) of the Isomers for the $C_2N^+ + H_2S$ Reaction at Singlet

species	B3LYP/6-311G(d,p)	CCSD(T)/6-311G(2df,p)	CCSD(T)/6-311G(2df,p) + ΔZPVE
1	−529.9249547/(−78.3)	−529.1627082/(−76.1)	−72.2
2	−530.0415510/(−151.5)	−529.2808043/(−150.2)	−143.5
2′	−530.0411143/(−151.2)	−529.2800018/(−149.7)	−143.0
3	−530.0154683/(−135.1)	−529.2476621/(−129.4)	−123.6
3′	−530.0151864/(−134.9)	−529.2473077/(−129.1)	−123.4
3″	−528.5221534/(−111.0)[a]	−529.2393829/(−124.2)	−118.4
4	−530.0561388/(−160.6)	−529.2969823/(−160.3)	−152.9
5	−530.0399517/(−150.4)	−529.2809948/(−150.3)	−142.1
5′	−530.0455749/(−154.0)	−529.2866384/(−153.8)	−145.6
6	−529.9133923/(−71.0)	−529.1496254/(−67.9)	−65.0
7	−530.0199605/(−137.9)	−529.2566433/(−135.0)	−128.7
7′	−530.0198057/(−137.8)	−529.2562117/(−134.7)	−128.4
8	−529.9911795/(−119.8)	−529.2265034/(−116.1)	−110.9
8′	−529.9858802/(−116.5)	−529.2215458/(−113.0)	−108.1
9	−530.0429744/(−152.3)	−529.2846119/(−152.6)	−147.3
10	−529.9734717/(−108.7)	−529.2095155/(−105.4)	−97.8
10′	−528.5046014/(−100.0)[a]	−529.2087720/(−105.0)	−97.2
11	−530.0726879/(−171.0)	−529.3066019/(−166.4)	−158.4
12	−529.8644026/(−40.3)	−529.0983859/(−35.7)	−33.3
13	−529.8959979/(−60.1)	−529.1298736/(−55.5)	−49.7
14	−529.9779614/(−111.5)	−529.2108326/(−106.3)	−100.6
14′	−529.9752535/(−109.9)	−529.2092415/(−105.3)	−99.8
15	−529.9849319/(−115.9)	−529.2213200/(−112.9)	−104.8
16	−530.0263809/(−141.9)	−529.2602212/(−137.3)	−130.1
17	−530.0220567/(−139.2)	−529.2608500/(−137.6)	−131.2
17′	−530.0212866/(−138.7)	−529.2598458/(−137.0)	−130.5
18	−529.9668714/(−104.6)	−529.2060817/(−103.3)	−97.2
19	−529.9363337/(−85.4)	−529.1739558/(−83.1)	−77.5
20	−529.9616667/(−101.3)	−529.2082101/(−104.6)	−99.3
21	−530.0185969/(−137.0)	−529.2656271/(−140.6)	−133.5
22	−529.9646750/(−103.2)	−529.2144116/(−108.5)	−101.8
22′	−529.9652165/(−103.6)	−529.2147454/(−108.7)	−102.1
23	−529.8917798/(−57.5)	−529.1322434/(−56.9)	−53.5
24	−529.9739337/(−109.0)	−529.2247678/(−115.0)	−107.3
25	−529.8979761/(−61.4)	−529.1555399/(−71.6)	−64.7
26	−529.9661697/(−104.2)	−529.2103299/(−105.9)	−98.3
27	−529.9774381/(−111.2)	−529.2242234/(−114.7)	−107.1
28	−529.9986725/(−124.5)	−529.2406193/(−125.0)	−116.5
29	−529.9702620/(−106.7)	−529.2146440/(−108.7)	−101.9
30	−530.0476732/(−155.3)	−529.2790963/(−149.1)	−140.6
31	−529.9873963/(−117.5)	−529.2320764/(−119.6)	−112.1
32	−529.9417769/(−88.8)	−529.1946617/(−96.1)	−88.9
33	−529.8713135/(−44.6)	−529.1217235/(−50.3)	−42.8
I	−530.0427432/(−152.0)	−529.2905478/(−156.3)	−151.0
II	−530.0197986/(−137.8)	−529.2668598/(−141.6)	−136.6

[a] Total and relative energies calculated at HF/6-311G(d,p) level.

The charge-transfer process of the title reactions has been considered. For the main reaction channel **Path R_1P_3**: $\mathbf{R_1} \rightarrow H_2SCCN^+$ (**1**) → $HSC(H)CN^+$ (**2**) → $SC(H)CNH^+$ (**4**) → $\mathbf{P_3}$ ($HCS^+ + HNC$), two charge-transfer types can be included: one is a direct process from $CCN^+ + H_2S$ to $CCN + H_2S^+$; the other is between the dissociation products such as $HCS^+ + HCN$ to $HCS + HCN^+$. The calculations for both possibilities are carried out at the CCSD(T)/6-311G(2df,p)//B3LYP/6-311G-(d,p) level. It can be seen that the relative energy of $CCN + H_2S^+$ is 9.3 kcal/mol lower than the reactants $\mathbf{R_1}$ ($CCN^+ + H_2S$) while that of $HCS + HCN^+$ is 99.4 kcal/mol higher than the final products $\mathbf{P_3}$ ($HCS^+ + HCN$). Namely, the direct charge-transfer process between the reactants is much feasible energetically than that between dissociation products.

Figure 4b shows the isomerization and dissociation pathways for the $\mathbf{R_2}$ ($CNC^+ + H_2S$) reaction. Generally, nearly all the pathways similar to those for the $\mathbf{R_1}$ ($CCN^+ + H_2S$) reaction can be located despite the quantitative differences that govern the overall reaction mechanism. For simplicity, we decide not to present the detailed similarities and discrepancies of the pathways for the two reactions. We can find that for the $\mathbf{R_2}$ ($CNC^+ + H_2S$) reaction, the most important pathways (underlined) starting from the initial adduct H_2SCNC^+ (**6**) may be written as

Path R_2P_3: $\mathbf{R_2} \rightarrow H_2SCNC^+$ (**6**) → $HSC(H)NC^+$ (**7**) → $HSC(H)NC^+$ (**7′**) → $HSC(H)CN^+$ (**2′**) → $HSC(H)CN^+$ (**2**) → $SC(H)CNH^+$ (**4**) → $\mathbf{P_3}$ ($HCS^+ + HNC$)

Path R_2P_2: $\mathbf{R_2} \rightarrow H_2SCNC^+$ (**6**) → $HSC(H)NC^+$ (**7**) → $HSC(H)NC^+$ (**7′**) → $HSC(H)CN^+$ (**2′**) → $HSC(H)CN^+$ (**2**) → $SC(H)CNH^+$ (**4**) → $\mathbf{P_2}$ ($HCS^+ + HCN$)

Path R_2P_1: $\mathbf{R_2} \rightarrow H_2SCNC^+$ (**6**) → $HSC(H)NC^+$ (**7**) → $HSC(H)NC^+$ (**7′**) → $HSC(H)CN^+$ (**2′**) → $HSC(H)CN^+$ (**2**) → $SC(H)CNH^+$ (**4**) → $SCC(H)NH^+$ (**5**(**5′**)) → $\mathbf{P_1}$ ($HCNH^+ + CS$)

TABLE 3: Total (au) and Relative Energies in Parentheses (kcal/mol) as Well as Those Including Zero-Point Vibration Energies (kcal/mol) of the Transition States for the $C_2N^+ + H_2O$ Reaction at Singlet

species	B3LYP/6-311G(d)	CCSD(T)/6-311G(2df,p)	CCSD(T)/6-311G(2df,p) + ΔZPVE
TS1/2	−529.8899091/(−56.3)	−529.1281504/(−54.4)	−52.5
TS1/3	−529.8620450/(−38.8)	−529.1018802/(−37.9)	−36.5
TS1/P$_4$	−529.8699563/(−43.8)	−529.1067246/(−40.9)	−40.4
TS2/2′	−529.9782665/(−111.7)	−529.2127270/(−107.4)	−102.8
TS2/3″	−529.8920260/(−57.6)	−529.1295693/(−55.3)	−53.3
TS2/4	−529.9576306/(−98.8)	−529.2008304/(−100.0)	−96.3
TS2/P$_6$	−529.8504901/(−31.6)	−529.0945209/(−33.3)	−32.6
TS2′/3′	−529.8958519/(−60.0)	−529.1332262/(−57.6)	−55.4
TS2′/7′	−529.9478371/(−92.6)	−529.1881618/(−92.0)	−87.0
TS2′/18	−529.8727518/(−45.5)	−529.1132068/(−45.0)	−42.5
TS2′/P$_4$	−529.9314502/(−82.4)	−529.1701902/(−80.8)	−77.8
TS2′/P$_6$	−529.8586582/(−36.7)	−529.1028317/(−38.5)	−37.4
TS3/4	−529.9538984/(−96.5)	−529.1863193/(−90.9)	−87.6
TS3″/5	−529.8556767/(−34.8)	−529.0941717/(−33.1)	−29.8
TS3″/5′	−529.8699911/(−43.8)	−529.1115554/(−44.0)	−40.2
TS4/5	−529.9769343/(−110.9)	−529.2122758/(−107.2)	−102.6
TS4/5′	−529.9813467/(−113.7)	−529.2146158/(−108.6)	−104.2
TS4/20	−529.9481321/(−92.8)	−529.1918831/(−94.4)	−89.1
TS4/P$_2$	−529.9557403/(−97.6)	−529.1922411/(−94.6)	−90.7
TS5/17	−529.9167497/(−73.3)	−529.1591148/(−73.8)	−70.4
TS5/30	−529.9386558/(−86.9)	−529.1703255/(−80.8)	−77.6
TS5/P$_2$	−529.9184962/(−74.2)	−529.1555269/(−71.6)	−67.2
TS6/7	−529.8718983/(−45.0)	−529.1084417/(−42.0)	−40.8
TS6/8	−529.8425489/(−26.6)	−529.0804911/(−24.5)	−23.5
TS6/P$_5$	−529.8512347/(−32.0)	−529.0869284/(−28.5)	−28.7
TS7/7′	−529.9685629/(−105.7)	−529.2039559/(−101.9)	−97.3
TS7/8′	−529.8594034/(−37.2)	−529.0961440/(−34.3)	−33.0
TS7/9	−529.9340618/(−84.0)	−529.1758490/(−84.3)	−79.9
TS7′/8	−529.8640846/(−40.1)	−529.0998751/(−36.6)	−35.2
TS7′/P$_5$	−529.9047146/(−65.6)	−529.1409846/(−62.4)	−59.8
TS8/8′	−529.9155385/(−72.4)	−529.1598628/(−74.3)	−72.2
TS8/9	−529.9318473/(−82.6)	−529.1685595/(−79.7)	−77.2
TS8/23	−529.8877658/(−55.0)	−529.1246113/(−52.2)	−49.9
TS8/P$_2$	−529.9220431/(−76.5)	−529.1701650/(−80.7)	−78.3
TS8′/11	−529.9260302/(−79.0)	−529.1644421/(−77.1)	−73.2
TS8′/P$_2$	−529.9269769/(−80.0)	−529.1728130/(−82.4)	−80.2
TS9/10	−529.9021134/(−64.0)	−529.1305449/(−55.9)	−52.7
TS9/10′	−529.9149031/(−72.0)	−529.1450530/(−65.0)	−61.7
TS9/P$_3$	−529.9310956/(−82.1)	−529.1719651/(−81.9)	−79.0
TS10/10′	−529.9257457/(−78.8)	−529.1651700/(−77.6)	−72.4
TS10/P$_1$	−529.9508143/(−94.5)	−529.1921850/(−94.6)	−88.4
TS10/P$_3$	−529.9270024/(−79.6)	−529.1658640/(−78.0)	−72.9
TS10′/P$_1$	−529.9372134/(−86.0)	−529.1762764/(−84.6)	−78.8
TS11/P$_1$	−529.9156353/(−72.4)	−529.1586699/(−73.5)	−71.6
TS11/P$_2$	−529.9302772/(−81.6)	−529.1687003/(−79.8)	−75.7
TS12/13	−529.8034801/(−2.1)	−529.0400421/(0.9)	1.6
TS12/14	−529.8080275/(−4.9)	−529.0494124/(−5.0)	−4.1
TS13/14′	−529.8070312/(−4.3)	−529.0400761/(0.9)	1.6
TS14/15	−529.8982346/(−61.5)	−529.1326069/(−57.2)	−54.2
TS14′/16	−529.9051193/(−65.8)	−529.1453291/(−65.2)	−61.8
TS15/16	−529.8706667/(−44.2)	−529.1063289/(−40.7)	−38.1
TS17/17′	−529.9901182/(−119.2)	−529.2295820/(−118.0)	−112.6
TS17′/P$_2$	−529.9191455/(−74.6)	−529.1568863/(−72.4)	−68.3
TS20/21	−529.8883501/(−55.3)	−529.1329311/(−57.4)	−54.7
TS21/27	−529.9644158/(−103.0)	−529.2078176/(−104.4)	−98.0
TS24/25	−529.8519950/(−32.5)	−529.1069884/(−41.1)	−36.8
TS28/P$_1$	−529.8493954/(−30.9)	−529.0916427/(−31.4)	−27.3

The **6** → **7** conversion is parallel to the **1** → **2** conversion for the **R$_1$** ($CCN^+ + H_2S$) reaction, whereas the steps starting from the isomer $HSC(H)CN^+$ (**2**) is the same as those in **Path R$_1$P$_3$**, **Path R$_1$P$_2$**, and **Path R$_1$P$_1$**.

In addition, there are two pathways

Path R$_2$P$_2$: **R$_2$** → H_2SCNC^+ (**6**) → $HSC(H)NC^+$ (**7**) → $SC(H)NCH^+$ (**9**) → **P$_2$** ($HCS^+ + HCN$)

Path R$_2$P$_3$: **R$_2$** → H_2SCNC^+ (**6**) → $HSC(H)NC^+$ (**7**) → $SC(H)NCH^+$ (**9**) → **P$_3$** ($HCS^+ + HNC$)

which are completely parallel to **Path R$_1$P$_3$** and **Path R$_1$P$_2$**, respectively. Yet, since the 1,4-H-shift transition state **TS7/9** (−79.9) is energetically much higher than the −CN ↔ −NC conversion transition state **TS2′/7′** (−87.0) and another 1,4-H-shift one **TS2/4** (−96.3), these two reaction pathways may be much less competitive than **Path R$_2$P$_3$**, **Path R$_2$P$_2$**, and **Path R$_2$P$_1$** in spite of their relative simplicity. The other pathways are kinetically much less probable. As a result, the feasibility order may be **Path R$_2$P$_3$** (major) > **Path R$_2$P$_1$** (minor) > **Path R$_2$P$_2$** (minor) for the **R$_2$** ($CNC^+ + H_2S$) reaction.

Hydrogen atom elimination is one of the most important channels for interstellar reaction, so the possibility of formation of products $SC_2NH^+ + H$ has been considered. The energetics calculated at the CCSD(T)/6-311G(2df,p)//B3LYP/6-311G(d,p)+ZPVE level for both **P$_9$** ($SC(H)CN^+ + H$) and **P$_{10}$** (SC-

TABLE 4: Harmonic Vibration Frequencies (cm^{-1}) for Singlet $C_2NH_2S^+$ Transition States at the B3LYP/6-311G(d,p) Level

species	harmonic vibration frequencies (cm^{-1})
TS1/2	−1526.4234, 173.3280, 248.0532, 484.1283, 545.4278, 597.5378, 885.8542, 948.1083, 1194.5508, 1971.6213, 2188.3945, 2375.9664
TS1/3	−1581.2151, 263.1903, 350.2831, 485.4089, 661.2999, 729.8911, 804.7178, 968.9417, 1064.5799, 1359.6603, 2021.2336, 2540.4289
TS1/P$_4$	−1505.2979, 164.2011, 22.0490, 438.5692, 492.3101, 675.3415, 733.0821, 749.2826, 1296.9157, 1726.2443, 2000.4146, 2149.9081
TS2/2′	−2152.2362, 186.6758, 254.1727, 499.1019, 601.9475, 790.1446, 967.5400, 1099.5356, 1322.4595, 2233.1024, 2520.9172, 3094.9104
TS2/3″	−1684.7086, 187.9353, 198.1961, 380.5188, 495.2266, 619.3109, 687.8172, 1000.9704, 1381.7997, 2008.8571, 2215.1064, 2473.4863
TS2/4	−1637.1166, 256.0294, 424.5890, 587.4405, 762.6691,873.6905, 960.9270, 999.3489, 1237.4526 1406.5558, 2160.3987, 3181.3874
TS2/P$_6$	−1133.2941, 108.8899, 152.6374, 350.9998, 416.9708, 502.8606, 613.2220, 866.9751, 1033.5438, 1860.8783, 2349.9279, 2547.5160
TS2′/3′	−1693.8059, 208.1110, 213.6246, 395.3447, 491.8283, 647.2509, 724.8443, 1020.3995, 37.3253, 2006.0475, 2188.5647, 2573.5545
TS2′/7′	−614.7625, 171.4288, 350.7146, 536.7052, 739.5577, 913.7467, 1002.0324, 1033.8216, 1317.0896, 1989.0327, 2600.7357, 3177.5174
TS2′/18	−1321.5769, 332.8049, 334.8548, 534.9664, 611.5335, 721.1894, 932.7144, 1047.7544, 1155.7074, 1519.6143, 2248.2497, 2595.1392
TS2′/P$_4$	−868.0252, 204.3706, 297.8176, 524.1278, 596.8996, 768.0134, 895.6972, 979.0104, 1370.4308, 1651.7464, 2316.7584, 2761.6442
TS2′/P$_6$	−1089.9579, 143.9560, 146.6424, 342.8205, 510.0834, 584.2850, 618.7397, 951.5377, 1061.1690, 1863.3742, 2328.6131, 2534.7367
TS3/4	−1690.4344, 182.4100, 207.7200, 425.5872, 520.6115, 646.3469, 685.3981, 808.5727, 1454.9863, 2068.5496, 2126.8700, 3492.8725
TS3″/5	−1297.4598, 91.8438, 284.4033, 646.2093, 769.5625, 852.5239, 861.5874, 1018.5487, 1169.5464, 1698.6776, 1805.1017, 3365.2040
TS3″/5′	−1360.8903, 203.6158, 416.3065, 589.6124, 776.2726, 900.9320, 937.0947, 999.4640, 1154.9866, 1670.9070, 1812.6810, 3485.5155
TS4/5	−1069.4632, 230.4773, 286.3246, 567.4863, 712.4398, 847.4315, 893.5360, 923.9164 1519.8647, 1933.6465, 2097.6132, 3451.8612
TS4/5′	−1212.2960, 244.2751, 280.3647, 569.6624, 684.1758, 727.9870, 914.6208, 990.5085 1514.7084, 1858.9118, 2124.2034, 3504.6464
TS4/20	−531.7654, 344.9813, 382.8964, 527.1292, 611.3831, 692.9520, 716.8053, 844.6437, 1005.0526, 2182.0368, 3074.7324, 3632.5153
TS4/P$_2$	−860.3065, 125.4341, 262.7754, 429.2444, 555.4405, 705.3742, 824.1665, 1123.2016, 1286.9073, 2005.7339, 2547.1275, 3140.8894
TS5/17	−1654.8672, 207.2702, 370.6183, 585.7080, 683.5805, 771.0482, 869.2856, 1129.3574, 1452.4114, 1682.5807, 1732.0794, 3182.2558
TS5/30	−2122.6483, 179.6978, 209.7612, 236.9400, 442.6675, 696.0310, 722.0050, 1118.0583, 1480.0481, 1858.3544, 2347.3042, 3258.3138
TS5/P$_2$	−863.8497, 120.1839, 287.9101, 559.5057, 728.3010, 880.6620, 960.3349, 1052.8962, 1288.0118 1690.6540, 2681.0894, 3124.7365
TS6/7	−1635.5507, 189.3287, 196.4309, 404.5575, 443.8387, 519.9368, 833.9023, 999.2094, 1240.8996, 1871.5075, 1979.4582, 2436.8661
TS6/8	−1563.4638, 244.5149, 362.2214, 431.6908, 600.8097, 691.7977, 830.1648, 981.8566, 1225.0539, 1356.3860, 1650.0919, 2584.8973
TS6/P$_5$	−1512.4994, 188.0096, 189.9260, 391.2824, 397.4920, 639.8596, 691.6756, 693.4900, 1315.2919, 1664.8345, 1956.7531, 2032.4567
TS7/7′	−1226.1346, 170.1979, 203.5485, 452.1080, 651.1606, 782.2509, 1017.5121, 207.0563, 1373.0544, 2023.6139, 2556.5150, 3094.1913
TS7/8′	−1313.8665, 104.5907, 211.3107, 352.9327, 443.1754, 651.1106, 667.2367, 980.9449, 1094.4985, 1759.7553, 2444.4553, 2489.4800
TS7/9	−1146.4454, 245.2816, 416.5255, 563.6884, 825.6015, 923.2626, 927.1885, 1122.6518, 1307.6183, 1799.3282, 2055.8539, 3177.3631
TS7′/8	−1339.7642, 108.1252, 214.2294, 363.5893, 441.9989, 648.8463, 688.1893, 996.3792, 1057.1379, 1766.1472, 2412.1883, 2614.8453
TS7′/P$_5$	−782.0561, 164.5649, 225.5736, 492.5530, 554.7494, 836.4324, 910.9636, 1063.8471, 1350.9277, 1888.5746, 2088.2823, 2569.2990
TS8/8′	−395.2900, 95.9980, 98.9171, 136.0761, 248.6321, 486.8093, 811.6187, 819.1988, 1019.2602, 2204.4885, 2429.9726, 3416.6655
TS8/9	−1774.7461, 207.4475, 222.5607, 405.8915, 481.0511, 503.6018, 731.9945, 804.1910, 1152.4283, 2071.6217, 2136.9802, 3363.7728
TS8/23	−766.8964, 207.7561, 259.0935, 522.3401, 555.3390, 654.5590, 792.6434, 1001.2720, 1107.6326, 1733.9891, 2395.4980, 2615.6364
TS8/P$_2$	−245.1272, 115.2194, 130.3653, 179.1202, 423.8287, 459.8687, 819.0299, 825.4473, 1150.6588, 2214.3726, 2256.5086, 3417.5763
TS8′/11	−1409.7367, 407.7929, 456.5781, 674.1374, 741.2976, 892.4237, 968.1703, 008.8707, 1418.7266, 1505.1005, 1781.1636, 3179.7061
TS8′/P$_2$	−510.8406, 116.6595, 117.7739, 198.4253, 390.5574, 435.0902, 819.3180, 827.4101, 1046.4669, 2199.8839, 2291.9154, 3407.5989

TABLE 4. (Continued)

species	harmonic vibration frequencies (cm^{-1})
TS9/10	−1437.4498, 209.3787, 256.1526, 459.9910, 674.4413, 754.4108, 861.5810, 914.3983, 1485.3585, 1857.8828, 1936.5336, 3108.9367
TS9/10′	−1477.2492, 252.9133, 264.0919, 480.3783, 628.9276, 746.4777, 961.2045, 1014.1766, 1436.9365, 1680.3750, 1959.1615, 3151.3953
TS9/P_3	−1268.7420, 113.5096, 229.0498, 299.2887, 380.2114, 655.6981, 799.8262, 1114.4171, 1315.6216, 1925.4350, 2280.9435, 3179.4021
TS10/10′	−1094.2015, 178.8937, 354.5480, 456.8618, 530.5542, 718.4636, 941.0407, 1238.8050, 1309.9471, 1883.6658, 2933.5758, 3370.5113
TS10/P_1	−569.5714, 142.1628, 200.2642, 555.0063, 688.2349, 880.8736, 997.6223, 1228.9763, 1424.9679, 1696.9474, 3218.9919, 3559.1299
TS10/P_3	−600.0369, 274.5280, 510.7539, 629.7441, 730.3102, 947.6719, 1001.6624, 1150.2606, 1498.4010, 1532.8585, 2227.7517, 3428.9701
TS10′/P_1	−641.4756, 182.9877, 211.0612, 562.4318, 679.5494, 702.9705, 887.2480, 1213.9187, 1418.7730, 1781.7577, 3230.4130, 3496.0828
TS11/P_1	−958.1317, 97.5955, 106.0464, 190.8066, 264.0842, 376.4847, 786.1034, 905.5904, 1383.4353, 1990.0294, 2303.0929, 3243.1753
TS11/P_2	−807.8793, 226.8015, 423.1041, 509.1058, 641.7002, 846.5537, 920.5542, 110.5731, 1348.4150, 1747.0172, 2250.7575, 3151.7146
TS12/13	−1152.9392, 143.1492, 189.7595, 219.1573, 298.2395, 444.2039, 604.1648, 900.9716, 1143.0421, 1935.2038, 2239.8986, 2641.8646
TS12/14	−1517.6797, 187.6925, 288.3644, 385.1080, 597.7992, 633.7287, 907.5665, 1017.6398, 1186.2057, 1324.1372, 1777.7453, 2572.3826
TS13/14′	−1948.4270, 66.9660, 173.2561, 174.8115, 406.6680, 542.5795, 652.3958, 1024.2596, 1189.7128, 1830.6857, 2220.5989, 2537.5031
TS14/15	−2041.3165, 195.1571, 253.6628, 419.5078, 514.8962, 621.6719, 778.0789, 820.3036, 1218.4384, 2051.8039, 2099.9056, 3398.2707
TS14′/16	−1543.6125, 350.4513, 443.0626, 539.0796, 743.1983, 796.8728, 908.8395, 914.6769, 1349.9425, 1443.9823, 1874.4354, 3315.7763
TS15/16	−1723.3672, 193.0908, 229.8642, 344.9166, 437.0345, 651.6923, 741.3376, 758.3481, 1268.0251, 2026.0949, 2077.5959, 3380.2305
TS17/17′	−595.0441, 355.0868, 359.4780, 558.8649, 879.5366, 943.5239, 969.6907, 1163.5033, 1354.9787, 1718.7697, 2603.6849, 3218.8237
TS17′/P_2	−1092.9046, 308.0894, 383.3292, 619.9738, 703.6819, 737.7561, 847.1136, 1047.2205, 1237.8152, 1725.5369, 2405.4082, 3189.4542
TS20/21	−1407.6041, 297.2167, 365.2354, 522.4178, 597.1909, 718.9888, 804.2961, 885.8739, 1119.2275, 1678.2793, 2175.2499, 3040.6267
TS21/27	−488.6187, 246.6030, 345.9318, 634.3360, 686.2385, 861.6644, 984.0593, 1105.9637, 1458.1566, 2145.0487, 3089.7891, 3230.9458
TS24/25	−1353.2846, 375.6667, 598.2241, 736.5900, 835.3582, 861.0769, 938.9061, 117.5441, 1223.1269, 1399.1516, 1965.7141, 3243.5268
TS28/P_1	−1225.5247, 352.8732, 439.0021, 587.0373, 668.5057, 697.1577 887.9787, 1072.0408, 1270.5402 1454.3534, 2433.4963, 3336.7638

(H)NC^+ + H) is listed in Table 1. It can be seen that energies of both products (−59.4 and −43.2 kcal/mol, respectively) are very higher than the corresponding isomer **2** (−143.5) and **7** (−128.7). Such product channels, i.e., **2** → **P_9** and **7** → **P_{10}**, are hardly achieved, which is in great agreement with the experimental studies by Bohme et al.[8]

It is of interest to point out that for both CXY^+ (XY = −CN or −NC) reactions, the 1,4-H-shift of H_2SCXY^+ (**1** or **6**) leading to $HSCXYH^+$ (**3** or **8**) is kinetically much less competitive than its 1,2-H-shift leading to $HSC(H)XY^+$ (**2** or **7**). Following the 1,2-H-shift adducts $HSC(H)XY^+$ (**2** or **7**), the same adduct SC(H)CNH^+ (**4**) can most probably be generated, which may lead to the final products **P_3** (HCS^+ + HNC), **P_1** ($HCNH^+$ + CS), and **P_2** (HCS^+ + HCN). To firm the most possible reaction mechanism mentioned here, total and relative as well as zero-point vibration energies of some most important isomers and transition states along the main reaction channels for the C_2N^+ + H_2S reaction have been calculated at the MP2/6-311G(d,p) level. The optimized geometries of these intermediates well agree with those calculated at the B3LYP/6-311G(d,p) level. The optimized structures are omitted for brevity and the energitics is listed in Table 5 for comparison.

3.1.3. Comparison with Experiments and Interstellar Implications. In section 3.1.2, we have obtained the most important pathways, i.e., **Path R_1P_3**, **Path R_1P_2**, and **Path R_1P_1** for the **R_1** (CCN^+ + H_2S) reaction, and **Path R_2P_3**, **Path R_2P_2**, and **Path R_2P_1** for the **R_2** (CNC^+ + H_2S) reaction. So, for both C_2N^+ reactions with H_2S, **P_3** (HCS^+ + HNC) may be the major product followed by the minor **P_1** ($HCNH^+$ + CS) and **P_2** (HCS^+ + HCN) (even less than **P_1**). Then reflected in the final product distributions, the $[H, C, S]^+$ mass spectrometric signal should be predominant over that of $HCNH^+$ for the CCN^+/CNC^+ + H_2S reactions. Signals of the other ions might be undetectably weak.

Considering the first two important isomers, the released heats of H_2SCCN^+ (**1**) (72.2 kcal/mol) and $HSC(H)CN^+$ (**2**) (143.5 kcal/mol) for the CCN^+ + H_2S reaction and those of H_2SCNC^+ (**6**) (40.3 kcal/mol) and $HSC(H)NC^+$ (**7**) (104.0 kcal/mol) for the CNC^+ + H_2S reaction are both very large. Thus, the CCN^+/CNC^+ + H_2S reactions are expected to be very fast, as is consistent with the rate constants 1.2×10^{-9} cm^3 $molecule^{-1}$ s^{-1} measured by Bohme et al.[8] for both of the reactions. But according to the PES shown in Figure 4a,b, the carbene reactivity (here referred to as the insertion into the S−H bond of H_2S) of the higher-energy CCN^+ is obviously greater than that of CNC^+, which is why the rate constants of the two reactions being equal should be questioned.

For the CCN^+ + H_2S reaction, only the rate constant was presented by Bohme et al.[8] using the SIFT technique, the distributions for the possible products were not given. In the

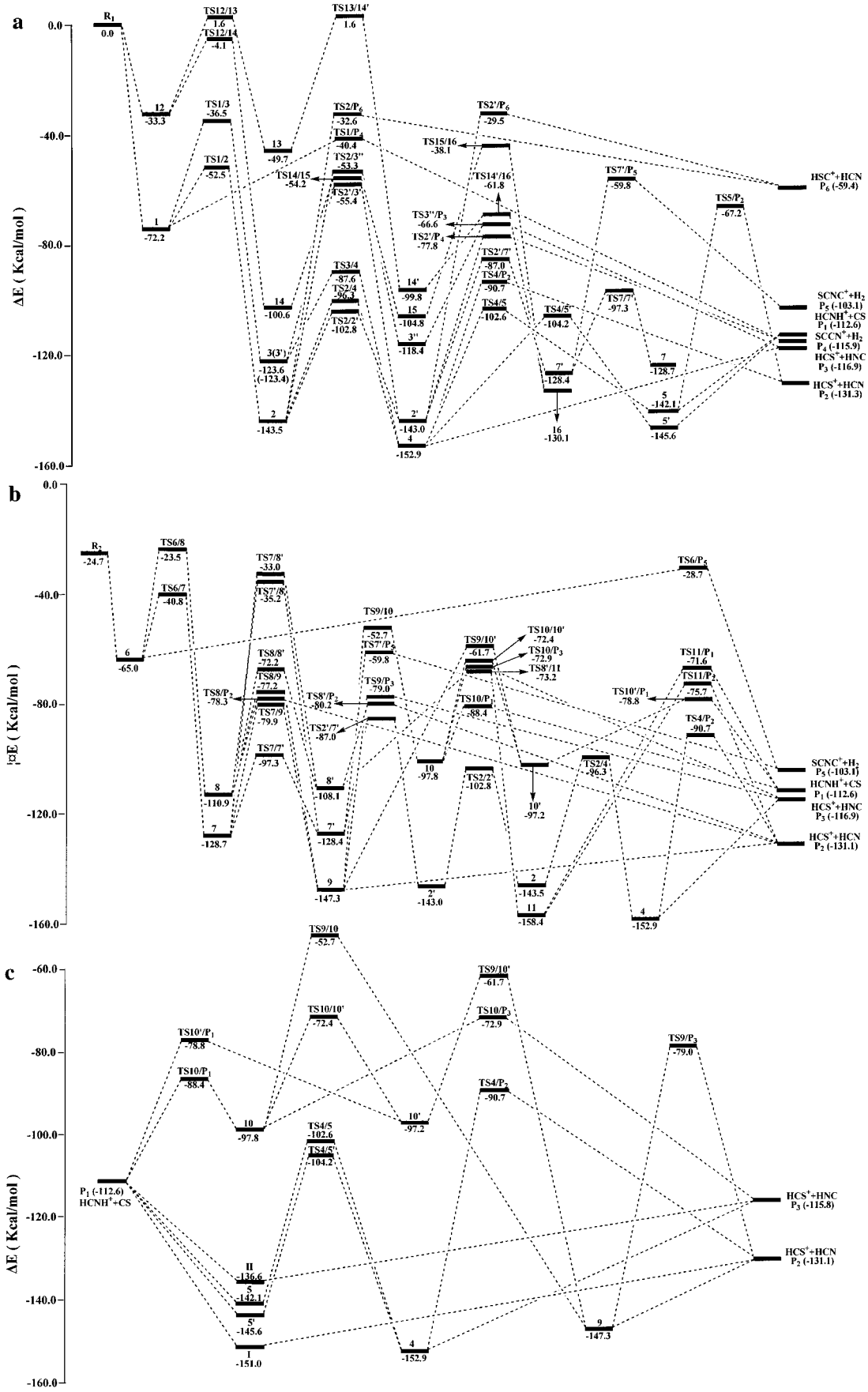

Figure 4. (a) Schematic pathways for the $CCN^+ + H_2S$ reaction. Relative energies are calculated at the CCSD(T)/6-311G(2df,p)//B3LYP/6-311G-(d,p)+ZPVE level. (b) Schematic pathways for the $CNC^+ + H_2S$ reaction. Relative energies are calculated at the CCSD(T)/6-311G(2df,p)//B3LYP/6-311G(d,p)+ZPVE level. (c) Schematic pathways for the $HCNH^+ + CS$ reaction. Relative energies are calculated at the CCSD(T)/6-311G(2df,p)//B3LYP/6-311G(d,p)+ZPVE level.

TABLE 5: Total (au) and Relative Energies in Parentheses (kcal/mol) as Well as Those Including Zero-Point Vibration Energies (kcal/mol) of Some Most Important Isomers and Transition States along the Main Reaction Channels for the $C_2N^+ + H_2S$ Reaction at Singlet by the MP2 Calculation

species	MP2/6-311G(d,p)	MP2/6-311G(d,p) + ΔZPVE
R_1	−528.8776850/(0.0)	0.0
R_2	−528.9045176/(−16.8)	−16.6
P_3	−529.0777414/(−125.5)	−121.9
1	−528.9939790/(−73.0)	−68.7
2	−529.1229383/(−153.9)	−147.1
2′	−529.1226578/(−153.7)	−146.9
4	−529.1358921/(−162.0)	−154.8
6	−528.9754680/(−55.1)	−51.6
7	−529.0886856/(−132.4)	−125.8
7′	−529.0885598/(−132.3)	−125.8
TS1/2	−528.9615142/(−52.6)	−50.3
TS2/2′	−529.0481485/(−107.0)	−102.1
TS2/4	−529.0391603/(−101.3)	−97.8
TS2′/7′	−529.0260566/(−93.1)	−87.8
TS6/7	−528.9355715/(−36.3)	−34.7
TS7/7′	−529.0327963/(−97.3)	−92.5

present article, the theoretical product distributions are obtained by ab initio calculations qualitatively. From the rich-energy reactants **R_1** ($CCN^+ + H_2S$), three most feasible channels are **Path R_1P_3**, **Path R_1P_1**, and **Path R_1P_2**, in which **Path R_1P_3** is the major product channel and **Path R_1P_1** and **Path R_1P_2** (even less than **Path R_1P_1**) are the minor ones. On the other hand, as shown in Figure 4a, the most feasible pathways for **P_4** ($SCCN^+ + H_2$) (−115.9) and **P_5** ($SCNC^+ + H_2$) (−103.1) can be written as

Path R_1P_4(1): $\mathbf{R_1} \rightarrow H_2SCCN^+$ (**1**) $\rightarrow$ HSC(H)CN^+ (**2**) $\rightarrow$ HSC(H)CN^+ (**2′**) $\rightarrow$ **P_4** ($SCCN^+ + H_2$)

Path R_1P_4(2): $\mathbf{R_1} \rightarrow H_2SCCN^+$ (**1**) $\rightarrow$ **P_4** ($SCCN^+ + H_2$)

Path R_1P_5: $\mathbf{R_1} \rightarrow H_2SCCN^+$ (**1**) $\rightarrow$ HSC(H)CN^+ (**2**) $\rightarrow$ HSC(H)CN^+ (**2′**) $\rightarrow$ HSC(H)NC^+ (**7′**) $\rightarrow$ **P_5** ($SCNC^+ + H_2$)

Because of the high barriers of **TS2′/P_4** (−77.8) and **TS7′/P_5** (−59.8), **Path R_1P_4(1)** and **Path R_1P_5** are surely much less competitive than **Path R_1P_1**, **Path R_1P_2** and **Path R_1P_3**. **Path P_4(2)** is even much less feasible due to the rather high-energy of **TS1/P_4** (−40.4). Namely, the formation of $C_2NS^+ + H_2$ may not be achieved for the kinetic factors. Notice that some of the secondary intramolecular proton transfer in **P_1** ($HCNH^+ + CS$) may give rise to the measured yields of **P_2** ($HCS^+ + HCN$) and **P_3** ($HCS^+ + HNC$).

The branching ratios of the $CNC^+ + H_2S$ reaction have been studied by Bohme et al. in the SIFT experiment.[8] Their observed product distributions were $CHS^+ + CHN$ (95%) and $C_2NS^+ + H_2$ (5%). Compared to our theoretical prediction that the $[H, C, S]^+$ mass spectrometric signal should be predominant over that of $HCNH^+$, the agreement is reasonably good. The final product $CH_2N^+ + CS$ may have little contribution to the whole reaction mechanism because the secondary intramolecular proton-transfer of **P_1** ($HCNH^+ + CS$) may lead to **P_2** ($HCS^+ + HCN$) and **P_3** ($HCS^+ + HNC$) before the fragments completely separate. Seen form the PES in Figure 4b, the generation of **P_4** ($SCCN^+ + H_2$) and **P_5** ($SCNC^+ + H_2$) may be less favorable due to the kinetic factors. Thus, the weak mass spectrometric signal of C_2NS^+ (5%) may be obtained from other source.

In the experiment by Bohmeet al.,[8] the actual chemical structure of the observed ion was uncertain. Our calculations show that for both C_2N^+ reactions, the HCS^+ ion instead of HSC^+ can be very efficiently formed, pointing to the significance of such rapid reactions for the HCS^+ abundance in interstellar space. However, C_2NS^+ may have undetectably low yields. Thus, it is difficult to synthesize the $SCCN^+$ or $SCNC^+$ species via the $C_2N^+ + H_2S$ reactions in dense clouds, which is somewhat agreeable to Bohme et al.'s proposal.[8] Moreover, it has been predicted that the CNC^+ and CCN^+ ions can be selectively generated in interstellar space via the scheme $C^+ + HCN/HNC \rightarrow CNC^+/CCN^+ + H$.[5] While the present theoretical study indicates the major dissociation channel as $CNC^+/CCN^+ + H_2S \rightarrow HCS^+ + HNC$ (not HCN), the successive $C^+ + HCN$ and $CNC^+ + H_2S$ reactions may be very effective loss processes of the HCN species and may provide a means for the isomerization of HCN to HNC. However, the $C^+ + HNC$ reaction is not an efficient process to consume HNC because the formed CCN^+ ion can rapidly react with H_2S to well recycle HNC.

To our best knowledge, this is the first theoretical investigation on the C_2N^+ reactions. The calculated potential energy surfaces may be very useful for future studies on the mechanisms of the other analogous C_2N^+ reactions such as those with H_2O, CH_4, NH_3, CH_3OH, CH_3OCH_3, etc.

3.2. Reactions of $HCNH^+$ with CS. The ion−molecule reaction of $HCNH^+$ with CS has not been the subject of previous investigations either experimentally or theoretically, although both species are very important in interstellar space. Two types of channels are considered for this reaction, i.e., proton transfer and association-elimination.

As shown in Figure 4c, the proton-transfer processes between $HCNH^+$ and CS can proceed barrierlessly to form the lowest-lying product **P_2** ($HCS^+ + HCN$) and **P_3** ($HCS^+ + HNC$) via low-lying hydrogen-bound complexes, i.e., SCH···NCH^+ (**I**) and SCH···CNH^+ (**II**), as illustrated by the dissociation curves of **I** and **II**. For simplicity, we just present the dissociation curve of the hydrogen-bound complex SCH···NCH^+ (**I**) to product **P_1** ($HCNH^+ + CS$) (Figures 5a and 6a) and to product **P_2** ($HCS^+ + HCN$) (Figures 5b and 6b) at both the B3LYP/6-311G(d,p) and single-point CCSD(T)/6-311G(2df,p) levels. Because the least stabilization energies of **I** and **II** are 38.4 and 24.0 kcal/mol, respectively, below **P_1**, such complexes may have a certain lifetime in low-temperature interstellar space. Particularly, since both CS and $HCNH^+$ have been proposed to have very large abundances in dense interstellar clouds,[1,2] such hydrogen-bound complexes are expected to be of great significance. Moreover, under the conditions with good-cage effect, the species HNC can be converted to its lower-energy HCN, respectively, with no barrier via the complexes as in the following exemplified pathway:

$$HCS^+ + HNC \rightarrow SCH\cdots NCH^+ (\mathbf{II}) \rightarrow HCNH^+ + CS \rightarrow SCH\cdots CNH^+ (\mathbf{I}) \rightarrow HCS^+ + HCN$$

Then, the HCN $\leftrightarrow$ HNC interconversion can be effectively realized via the so-called "proton transport" or "back and forth" catalysis mechanism.[17,18]

The attack of the C-atom of CS at the C-atom of $HCNH^+$ can barrierlessly lead to the low-lying adducts; the formed SCC(H)NH^+ (**5** and **5′**) lie 29.5 and 33.0 kcal/mol below the corresponding reactants. The very lower-energy isomer SC(H)CNH^+ (**4**) can be formed via two 1,2-H-shift transition states between the adjacent C-atom **TS4/5** (−102.6) and **TS4/5′** (−104.2), followed by the direct dissociation to the final product **P_3** ($HCS^+ + HNC$). Also, **4** can disassociate to **P_2** ($HCS^+ +$

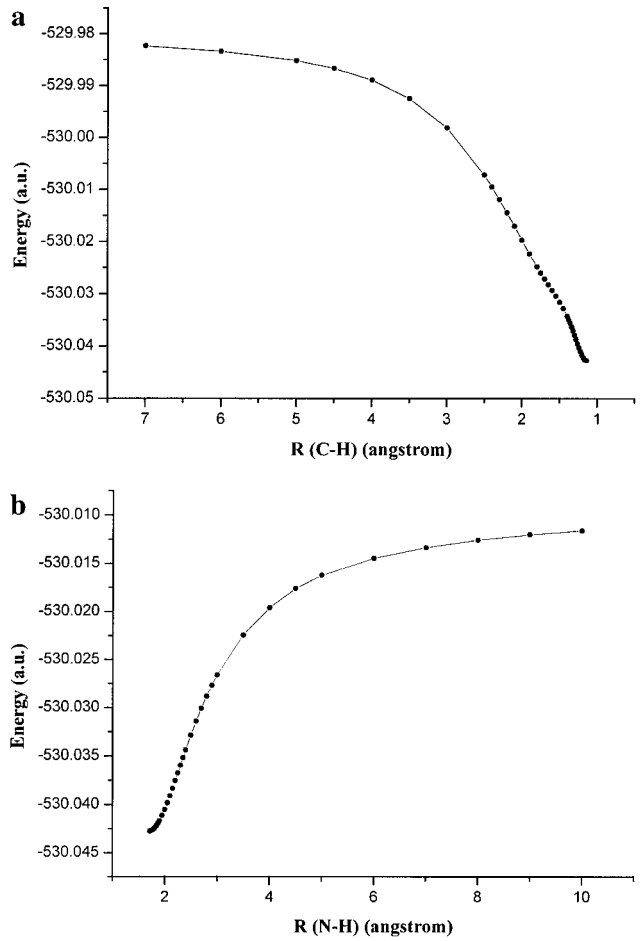

Figure 5. (a) Dissociation curve of the hydrogen-bound complex SCH···NCH^+ (**I**) to product $\mathbf{P_1}$ ($HCNH^+ + CS$) with reference to the internal C−H bond at the B3LYP/6-311G(d,p) level. (b) Dissociation curve of the hydrogen-bound complex SCH···NCH^+ (**I**) to product $\mathbf{P_2}$ ($HCS^+ + HCN$) with reference to the internal N−H bond at the B3LYP/6-311G(d,p) level. The calculations are performed by pointwise optimization of the remaining varied bond lengths with every fixed internal C−H or N−H bond lengths. During the optimization, the symmetry is constrained as $C_{\infty v}$.

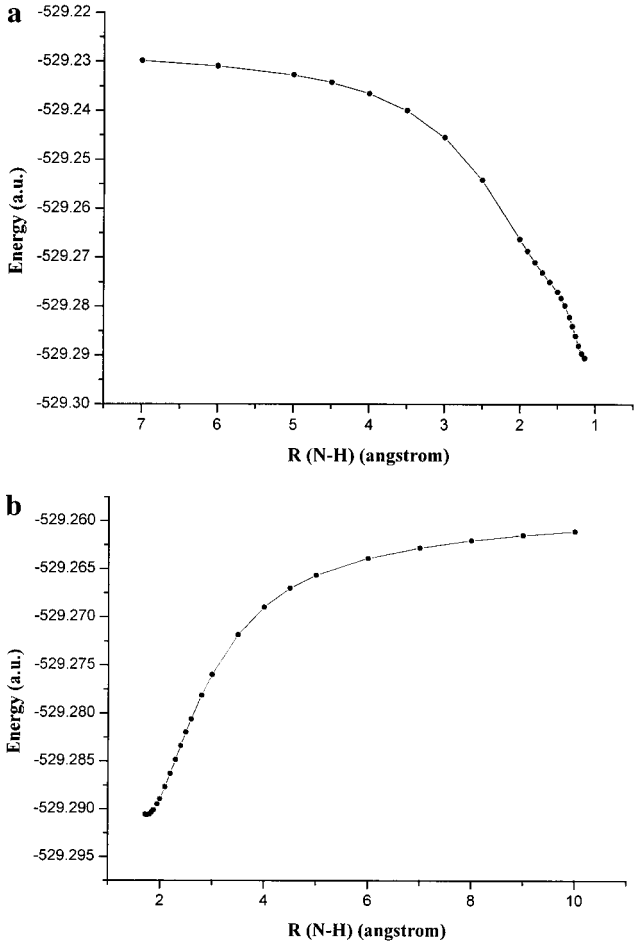

Figure 6. (a) Dissociation curve of the hydrogen-bound complex SCH···NCH^+ (**I**) to product $\mathbf{P_1}$ ($HCNH^+ + CS$) with reference to the internal C−H bond at the single-point CCSD(T)/6-311G(2df,p)//B3LYP/6-311G(d,p) level. (b) Dissociation curve of the hydrogen-bound complex SCH···NCH^+ (**I**) to product $\mathbf{P_2}$ ($HCS^+ + HCN$) with reference to the internal N−H bond at the single-point CCSD(T)/6-311G(2df,p)//B3LYP/6-311G(d,p) level.

HCN) via $\mathbf{TS4/P_2}$ (−90.7), but the existence of an energy barrier along the reaction pathway makes such a product channel much less competitive than the directly dissociated one.

Considerable barriers are needed when the C-atom of CS attacks the N-atom of $HCNH^+$ to form $SCN(H)CH^+$ (**10** (−97.8) and **10′** (−97.2)) via $\mathbf{TS10/P_1}$ and $\mathbf{TS10'/P_1}$, which lie 24.2 and 33.8 kcal/mol above the corresponding reactants $\mathbf{P_1}$ ($HCNH^+ + CS$). Even though the energy barriers along the following pathways:

$$SCN(H)CH^+ (\mathbf{10}\ (\mathbf{10'})) \rightarrow SC(H)NCH^+ (\mathbf{9}) \rightarrow \mathbf{P_2}\ (HCS^+ + HCN)$$

$$SCN(H)CH^+ (\mathbf{10}\ (\mathbf{10'})) \rightarrow SC(H)NCH^+ (\mathbf{9}) \rightarrow \mathbf{P_3}\ (HCS^+ + HNC)$$

are not considered, the initial barriers from the reactants $HCNH^+ + CS$ to **10** (**10′**) do not seem easy to overstep, which means that the pathways starting from the attacks of the C-atom of CS on the N-atom of $HCNH^+$ are energetically unfavorable compared with the attacks of the C-atom of CS on the C-atom $HCNH^+$. Due to significant barriers, the other isomerization and decomposition pathways are even inaccessible.

All in all, for the $HCNH^+ + CS$ reactions, the final products $HCS^+ + HCN/HNC$ can be generated by both the proton-transfer and the association-elimination processes. But the barrierless proton-transfer processes may well compete with the barrierless association-elimination one considering the height of energy barriers existing along the reaction pathways. Since it has not been studied experimentally, we hope our calculations may provide useful information for future laboratory investigations. For the $HCNH^+ + CS$ reaction as well as the $CCN^+/CNC^+ + H_2S$ reactions, the primary products HCS^+ and HNC discussed in this section may have some contribution to the relative abundances of the $HCNH^+$/HCN/HNC systems in interstellar space.

4. Conclusions

A detailed theoretical study at the CCSD(T)/6-311G(2df,p)//B3LYP/6-311G(d,p) level has been performed on the $CCN^+/CNC^+ + H_2S$ and $HCNH^+ + CS$ reaction mechanisms. The main results can be summarized as follows:

(1) The carbene insertion of CNC^+/CCN^+ into the S−H bond of H_2S can lead to the low-lying isomer $HSC(H)NC^+$ (**7**)/$HSC(H)CN^+$ (**2**) via the initial adduct H_2SCNC^+ (**6**)/H_2SCCN^+ (**1**). For the $CNC^+ + H_2S$ reaction, isomer **7** (**7′**) may take a −NC ↔ -CN conversion to give the low-lying isomer **2′** (**2**). Then,

for both C_2N^+ reactions, a 1,4-H-shift of **2** may lead to SC(H)CNH^+ (**4**). Finally, **4** may either directly dissociate to the major product $\mathbf{P_3}$ ($HCS^+ + HNC$) (much less $\mathbf{P_2}$ ($HCS^+ + HCN$)), or indirectly to the even less $\mathbf{P_1}$ ($HCNH^+ + CS$) via the low-lying intermediate SCC(H)NH^+ (**5** (**5′**)). Concerning the product distributions, our calculations may have some contributions to the further experimental observation in the future. The results reported in this paper may be the first theoretical study on the reaction of the two C_2N^+ isomeric ions. We hope that our computations may provide useful information for understanding the C_2N^+ carbene reactivity toward the other analogous neutral species such as H_2O, CH_4, NH_3, and CH_3-OH. The theoretical studies of such reactions are under way by our groups.

(2) For the $HCNH^+ + CS$ reactions, the proton transfer may barrierlessly lead to the final products $\mathbf{P_2}$ ($HCS^+ + HCN$) or $\mathbf{P_3}$ ($HCS^+ + HNC$) via the ion−molecule complexes SCH···NCH^+ (**I**) or SCH···CNH^+ (**II**), respectively, while the barrierless association-elimination may lead to the lower-energy adducts SCC(H)NH^+ (**5** (**5′**)), which may further dissociate to $\mathbf{P_3}$ ($HCS^+ + HNC$) by a H-shift between two adjacent C-atoms and dissociate directly process via isomer SC(H)CNH^+ (**4**). Such an ion−molecule reaction has not been previously investigated, and the present calculations are expected to stimulate future laboratory studies.

The title ion−molecule reactions are expected to have certain contribution to the relative abundance of the important $HCNH^+$/HCN/HNC systems observed in interstellar space.

Acknowledgment. This work is supported by the National Natural Science Foundation of China (No. 29892168, No. 20073014, No. 20103003), Doctor Foundation by the Ministry of Education, Foundation for University Key Teacher by the Ministry of Education, and Key Subject of Science and Technology by the Ministry of Education of China.

References and Notes

(1) Smith, D.; Spanel, P. *Mass. Spectrom. Rev.* **1995**, *14*, 25.

(2) Gerlich, D.; Horning, S. *Chem. Rev.* **1992**, *92*, 1509.

(3) Phillips, L. F. *Pro. Energy Combust. Sci.* **1992**, *18*, 75.

(4) Hartquist, T. W.; Dalgarno, A. *Proceedings of the Gregynog Conference on Giant Molecular Clouds*; Solomon, P., Ed.; Pergamon: New York, 1979.

(5) Mitchell, G. F.; Ginsberg, J. L.; Kuntz, P. J. *Astrophys. J. Suppl.* **1978**, *38*, 39.

(6) Harland, P. W.; McIntosh, B. J. *Int. J. Mass. Spectrom. Ion Processes* **1985**, *67*, 29.

(7) Harland, P. W. *Int. J. Mass. Spectrom. Ion Processes* **1986**, *70*, 231.

(8) Bohme, D. K.; Wlodek, S.; Raksit, A. B.; Schiff, H. I.; Mackay, G. I.; Keskinen, K. J. *Int. J. Mass. Spectrom. Ion Processes* **1987**, *81*, 123.

(9) McEwan, M. J., Anicich, V. G.; Huntress, W. T. *Int. J. Mass. Spectrom. Ion Phys.* **1983**, *50*, 179.

(10) Haese, N. N.; Woods, R. C. *Astrophys. J.* **1981**, *246*, L51.

(11) Yoshimine, M.; Kraemer, W. P. *Chem. Phys. Lett.* **1982**, *90*, 145.

(12) Peng, J. P.; Xu, X. H.; Marshall, P. *J. Phys. Chem. A* **1999**, *103*, 5307.

(13) Costen, M. L.; Hancock, G.; Ritchie, G. A. D. *J. Phys. Chem. A* **1999**, *103*, 10644.

(14) Costen, M. L.; Hancock, G.; Ritchie, G. A. D. *J. Phys. Chem. A* **1999**, *103*, 10651.

(15) Bohme, D. K. *Nature* **1986,** 319, 473.

(16) Frisch, M. J.; Trucks, G. W.; Schlegel, H. B.; Scuseria, G. E.; Robb, M. A.; Cheeseman, J. R.; Zakrzewski, V. G.; Montgomery, J. A., Jr.; Stratmann, R. E.; Burant, J. C.; Dapprich, S.; Millam, J. M.; Daniels, A. D.; Kudin, K. N.; Strain, M. C.; Farkas, O.; Tomasi, J.; Barone, V.; Cossi, M.; Cammi, R.; Mennucci, B.; Pomelli, C.; Adamo, C.; Clifford, S.; Ochterski, J.; Petersson, G. A.; Ayala, P. Y.; Cui, Q.; Morokuma, K.; Malick, D. K.; Rabuck, A. D.; Raghavachari, K.; Foresman, J. B.; Cioslowski, J.; Ortiz, J. V.; Stefanov, B. B.; Liu, G.; Liashenko, A.; Piskorz, P.; Komaromi, I.; Gomperts, R.; Martin, R. L.; Fox, D. J.; Keith, T.; Al-Laham, M. A.; Peng, C. Y.; Nanayakkara, A.; Gonzalez, C.; Challacombe, M.; Gill, P. M. W.; Johnson, B. G.; Chen, W.; Wong, M. W.; Andres, J. L.; Head-Gordon, M.; Replogle, E. S.; Pople, J. A. *Gaussian 98*, revision A.7; Gaussian, Inc.: Pittsburgh, PA, 1998.

(17) Chalk, A. J.; Radom, L. *J. Am. Chem. Soc.* **1997**, *119*, 9**,** 7573.

(18) Cunje, A.; Rodriguez, C. F.; Bohme, D. K.; Hopkinsor, A. C. *J. Phys. Chem. A* **1998**, *102*, 478.